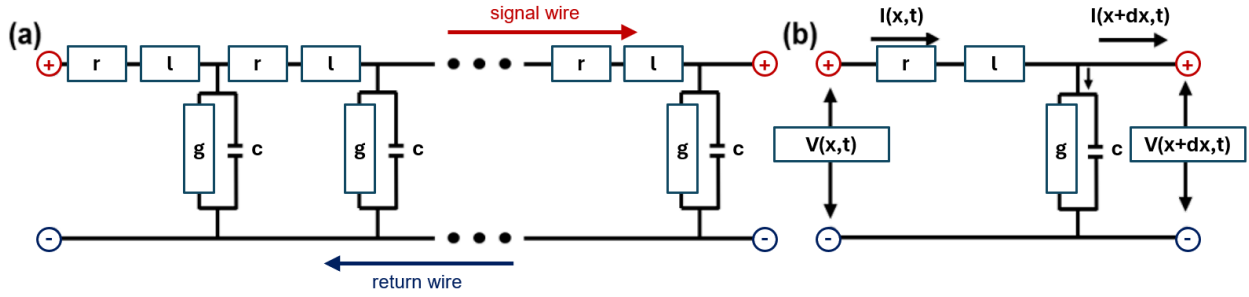


1  
2  
3  
4  
5  
6  
7  
8  
9  
10  
11  
12  
13  
14  
15  
16  
17  
18  
19  
20  
21  
22  
23  
24  
25  
26  
27  
28  
29  
30  
31  
32  
33  
34  
35  
36

**Supplementary Information**  
**Dissipative Charge Transport in Organic Mixed Ionic-Electronic Conductor**  
**Channels**

Filippo Bonafè<sup>1,†</sup>, Mattia Bazzani<sup>1,†</sup>, Beatrice Fraboni<sup>1</sup> and Tobias Cramer<sup>1,\*</sup>

37 **1. Transmission line theory**  
 38



**Figure S1. Electrical transmission lines.** (a) Circuitual representation of a transmission line. Propagating voltages are applied between the “signal” wire (labelled with a “+” sign) and the “return” wire (labelled with a “-” sign) constituting the line. The electrical properties of the system are modelled using repeated transmission line elements (b). The entire transmission line can be treated as the result of infinite subsequent transmission line elements.

39 The propagation of electrical signals along a transmission line is typically described using the  
 40 telegrapher’s equation.<sup>1</sup> In this approach, the transmission line is assumed to be composed of an  
 41 infinite series of elementary components specified per unit length (Figure S1a), each representing  
 42 an infinitesimally short segment of the line (Figure S1b):

- 43 • The distributed resistance  $r$  of the line is represented by a series resistor (expressed  
 44 in ohms per unit length).
- 45 • The distributed inductance  $l$  (due to the magnetic field around the wires, self-inductance,  
 46 etc.) is represented by a series inductor (henries per unit length).
- 47 • The capacitance  $c$  between the “signal” wire and the “return” wire constituting the line in  
 48 Figure S1 is represented by a shunt capacitor (farads per unit length).
- 49 • The conductance  $g$  of the material separating the two wires is represented by a shunt  
 50 resistor (siemens per unit length).  $r_{shunt} = 1/g$  accounts for current leakage processes  
 51 occurring at the interface between the two wires (also known as dielectric losses if the  
 52 conductors constituting the line are separated by a dielectric material).

53 Under these assumption, the variation of current  $I(x,t)$  and voltage  $V(x,t)$  on time and space can  
 54 be modeled using the Telegrapher’s equations<sup>1</sup>

55 
$$\frac{\partial V(x,t)}{\partial x} = -r \cdot I(x,t) - l \cdot \frac{\partial I(x,t)}{\partial t} \quad (S1)$$

56 
$$\frac{\partial I(x,t)}{\partial x} = -g \cdot V(x,t) - c \cdot \frac{\partial V(x,t)}{\partial t} \quad (S2)$$

57 Eq. S1 and S2 can be turned into single-variable differential equations in the frequency domain,  
 58 considering  $V(x,t) = \text{Re}\{\bar{V}(x)e^{j\omega t}\}$  and  $I(x,t) = \text{Re}\{\bar{I}(x)e^{j\omega t}\}$  (with  $\bar{V}(x)$  and  $\bar{I}(x)$  voltage and  
 59 current phasors)

$$60 \quad \frac{d^2\bar{V}(x)}{dx^2} - \gamma^2\bar{V}(x) = 0 \quad (\text{S3})$$

$$61 \quad \frac{d^2\bar{I}(x)}{dx^2} - \gamma^2\bar{I}(x) = 0 \quad (\text{S4})$$

62 which are solved by

$$63 \quad \bar{V}(x) = \bar{V}_0^+ e^{-\gamma x} + \bar{V}_0^- e^{\gamma x} \quad (\text{S5})$$

$$64 \quad \bar{I}(x) = \bar{I}_0^+ e^{-\gamma x} - \bar{I}_0^- e^{\gamma x} \quad (\text{S6})$$

65 where the "+" and "-" superscripts label respectively forward and backward travelling waves, and  
 66  $\gamma$  is introduced as propagation constant

$$67 \quad \gamma = \alpha + j\beta = \sqrt{\frac{Z_{line}}{Z_{transversal}}} = \sqrt{(r + j\omega l)(g + j\omega c)} \quad (\text{S7})$$

68 The coefficients  $\alpha$  and  $\beta$  in Eq. S7 represent respectively the attenuation coefficient and the phase  
 69 constant coefficient indicating how much the signal amplitude gets attenuated and the phase  
 70 changes with distance. The determination of  $\beta$  at different frequencies provides the dispersion  
 71 relation of the material. An analytical expression for the dispersion relation provides knowledge  
 72 on the signal propagation velocity inside of the material and of its dependence on frequency. In  
 73 fact, the phase velocity of a travelling wave is given by

$$74 \quad v_{phase} = \frac{\omega}{\beta} \quad (\text{S8})$$

75 while the propagation velocity of a wave packet can be calculated as

$$76 \quad v_{group} = \frac{\partial\omega}{\partial\beta} \quad (\text{S9})$$

77

78

79

80

81

82

83 **2. Cable equation for OMIEC materials**

84

85 The cable equation S3 can be solved for the transmission line presented in Figure 2a describing  
 86 the OMIEC/electrolyte interface. When a sinusoidal signal  $V_{in}(t) = \text{Re}\{V_{in} e^{j\omega t}\} = \text{Re}\{\bar{V}_{in}\}$  is  
 87 injected in the OMIEC electrode from a metallic contact (see Figure 2a), the solution S5 becomes

88 
$$V(x, t) = (Ae^{-\gamma x} + Be^{\gamma x})e^{j\omega t} \quad (\text{S10})$$

89 or, in the phasor formalism

90 
$$\bar{V}(x) = Ae^{-\gamma x} + Be^{\gamma x} \quad (\text{S11})$$

91 where the phase of the propagating wave is determined by  $A$  and  $B$  coefficients. These can be  
 92 calculated by imposing boundary conditions. If the propagated potential in  $x = 0$  is equal to the  
 93 input signal  $V_{in}(t)$ , and the potential is constant at the end of the channel ( $x = L$ ), we write

94 
$$\bar{V}(x = 0) = \bar{V}_{in} \quad (\text{S12})$$

95 
$$\left. \frac{d\bar{V}}{dx} \right|_{x=L} = 0 \quad (\text{S13})$$

96 We obtain

97 
$$A = \frac{\bar{V}_{in}}{1 + e^{-2\gamma L}} ; \quad B = \frac{\bar{V}_{in}e^{-2\gamma L}}{1 + e^{-2\gamma L}} \quad (\text{S14})$$

98 and

99 
$$\bar{V}(x) = \frac{\bar{V}_{in}}{1 + e^{-2\gamma L}} [e^{-\gamma x} + e^{\gamma(x-2L)}] \quad (\text{S15})$$

100 which is the equivalent of Eq. 4 in the complex plane. The total current flowing from the OMIEC  
 101 channel into the surrounding electrolyte is given by

102 
$$\bar{I}(L) = \int_0^L \frac{\bar{V}(x)}{z_0} dx = \frac{\bar{V}_{in}}{\sqrt{r_0 z_0}} \tanh(\gamma L) \quad (\text{S16})$$

103 Finally, considering that the impedance is defined as the transfer function correlating the input  
 104 voltage  $\bar{V}_{in}$  and the output current  $\bar{I}(L)$ , we obtain for the vertical ionic transport

105 
$$Z(L) = \frac{\bar{V}_{in}}{\bar{I}(L)} = \sqrt{r_0 z_0} \coth(\gamma L) \quad (\text{S17})$$

106 corresponding to the De Levie impedance originally derived for “porous” electrodes.<sup>2</sup> Ultimately,  
 107 as both faradaic processes and inductive effects are negligible in our experiments, we can set  $g=l=0$   
 108 in Eq. S7. The propagation constant can be thus defined as in Eq. 3 where we only consider  
 109 electronic transport along the OMIEC channel and capacitive ionic charging of the material bulk.

### 110 3. Signal propagation spectroscopies at different doping level

111

112 Signal propagation spectroscopies acquired at different DC offset voltages demonstrate that lower  
113 doping levels induce signal attenuation at lower frequencies (Fig. S3a), and cause a larger  
114 dispersion (Fig. S3b) in the travelling potential. Data (indicated with small squares) can be fitted  
115 with Eq. 4 (continuous lines) to obtain the electronic conductivity, the ionic conductivity, and the  
116 volumetric capacitance  $c_v$  of PEDOT:PSS at different electrochemical potentials. Results are  
117 reported in Figure 3g

118

119

120

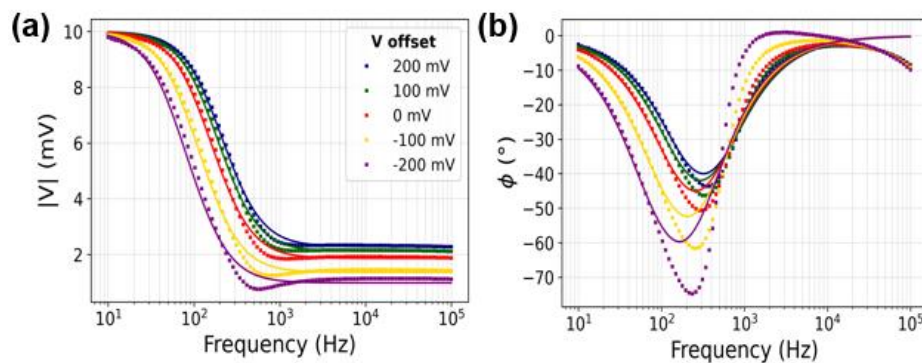
121

122

123

124

125



126 **Figure S3. Signal propagation spectroscopies at different doping levels.** a) Amplitude and  
127 phase (b) spectra of propagating AC signals collected at a distance  $L=640 \mu\text{m}$  from the injecting  
128 contact, showing increased dissipation for lower doping levels.

129

130

131

132

133

134

135

136

137

138

139

140

141 **4. Determination of PEDOT:PSS electronic conductivity from OECT measurements**

142

143 The electronic conductivity of PEDOT:PSS was calculated from the DC transfer characteristics of  
144 an organic electrochemical transistor (OECT) (Figure S4) using the equation

145 
$$\sigma_{el} = \frac{I_{D,DC}L}{V_{D,DC}Wt_h} \quad (S18)$$

146 where  $I_{D,DC}$  is the drain current and  $V_{D,DC}$  the applied drain voltage.

147

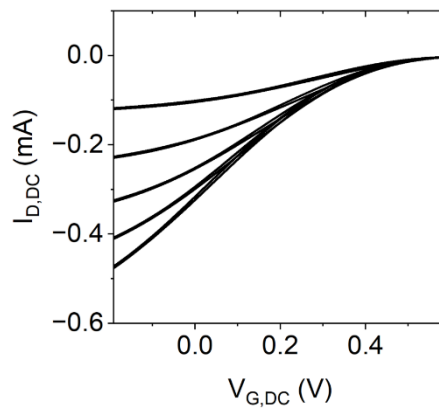


**Figure S4. OECT transfer characteristics.** The PEDOT:PSS channel has dimensions  $W = L = 30$   $\mu\text{m}$ . An Ag/AgCl wire was used as gate to modulate the channel conductivity. Electronic conductivities reported in Figure 3e were calculated from data acquired with  $V_{D,DC} = -0.1$  V.

148

149

150

151

152

153

154

155

156

157

158

159 **5. Dispersion relation in OMIEC materials**

160

161 Eq. 3 allows to calculate an analytical expression for the propagation constant as a function of the  
162 geometrical and electrical properties of the OMIEC thin film

$$163 \quad \gamma = \sqrt{\frac{r_0}{z_0}} = \sqrt{\frac{\omega^2 c_{vol}^2 \rho_{el} \rho_{ion} t^2}{1 + \omega^2 c_{vol}^2 \rho_{ion}^2 t^4} + j \frac{\omega c_v \rho_{el}}{1 + \omega^2 c_{vol}^2 \rho_{ion}^2 t^4}} = \sqrt{A + jB} \quad (S19)$$

164 In the limit of infinite transmission line ( $L \rightarrow \infty$ ), the expression for the propagating potential S15  
165 assumes a simple form:

$$166 \quad \bar{V}(x, \omega) = \bar{V}_{in} e^{-\gamma(\omega)x} = \bar{V}_{in} e^{-[\alpha(\omega) + j\beta(\omega)]x} \quad (S20)$$

167 allowing to identify  $\alpha = \text{Re}(\gamma)$  as the attenuation coefficient and  $\beta = \text{Im}(\gamma)$  as the phase constant of  
168 the OMIEC channel satisfying:

$$169 \quad \alpha(\omega) = -\frac{1}{x} \ln \left[ \frac{|V(x, \omega)|}{|V_{in}|} \right]; \quad \beta(\omega) = -\frac{\phi(\omega, x)}{x} \quad (S21)$$

170 Under this assumption, we determine an analytical expression for the dispersion relation of the  
171 OMIEC material

$$172 \quad \beta(\omega) = \text{Im} \left( \sqrt{\sqrt{A^2 + B^2} e^{j \tan^{-1} \left( \frac{B}{A} \right)}} \right) = \sqrt[4]{A^2 + B^2} \sin \left[ \frac{\tan^{-1} \left( \frac{B}{A} \right)}{2} \right] \quad (S22)$$

173 where  $A$  and  $B$  are defined according to Eq. S19.

174 Eq. S21 allows to calculate the dispersion relation for the OMIEC material from the phase shift of  
175 the signal propagating in the PEDOT:PSS thin film. Results obtained at different channel sites  
176 from data in Figure 3c are reported in Figure S5. In this plot, the black continuous line represents  
177 the dispersion relation predicted by Eq. S22, and calculated using the experimental values of the  
178 transport parameters  $\rho_{el}$ ,  $\rho_{ion}$  and  $c_v$  obtained by fitting the potential signal propagation data.  
179 Experimental curves align well with the theoretical predictions, displaying similar curve shapes  
180 and frequencies at which maximum dispersion occurs. At the same time, despite the dispersion  
181 relation in Eq. S22 is independent from the position on the OMIEC channel, the acquired data  
182 traces do not completely overlap. Such a discrepancy occurs because Eq. S22 is only valid for an

183 infinite transmission line, while experimental measurements are affected by finite-length effects.  
184 According to this observation, data acquired in the farthest site from the injecting electrode ( $L =$   
185  $640 \mu\text{m}$ ) show a better agreement with the theoretical predictions.  
186

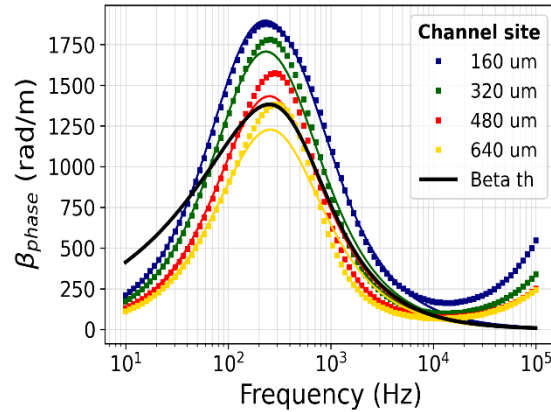


**Figure S5. Dispersion relation for a PEDOT:PSS channel.** Dots represent the experimental data, while solid lines result by fitting with Eq. 4 the signal propagation spectroscopies in Figure 3b and 3c. The theoretical dispersion relation (black line – valid for an infinite long channel) is calculated with the averaged parameters  $\rho_{el}$ ,  $\rho_{ion}$  and  $c_v$  resulting from the fits obtained at different channel positions.

187  
188  
189  
190  
191  
192  
193  
194  
195  
196  
197  
198  
199  
200  
201

202 **6. Low and high frequency limit for the propagation constant**

203

204 The propagation constant in Eq. 3 can be written as

205 
$$\gamma = \sqrt{\frac{r_0}{z_0}} = \sqrt{\frac{j\omega c_v \rho_{el}}{1 + j\omega c_v \rho_{ion} t_h^2}} = \sqrt{\frac{j\omega c_v \rho_{el} + \omega^2 c_v^2 \rho_{el} \rho_{ion} t_h^2}{1 + \omega^2 c_v^2 \rho_{ion}^2 t_h^4}} \quad (S23)$$

206 If we introduce  $\tau_{ion} = R_{ion} * C$  as the time constant for the ionic circuit (where  $R_{ion} = \frac{\rho_{ion} t_h}{WL}$  and

207  $C = c_v * L * W * t_h$  are the total ionic resistance and capacitance of the OMIEC thin film), the (angular)

208 ionic frequency cutoff is defined as

209 
$$\omega_c = \frac{1}{\tau_{ion}} = \frac{1}{c_v \rho_{ion} t_h^2} \quad (S24)$$

210 Eq. S23 can be rewritten as

211 
$$\gamma = \sqrt{\frac{j\omega c_v \rho_{el} + \omega^2 c_v^2 \rho_{el} \rho_{ion} t_h^2}{1 + \left(\frac{\omega}{\omega_c}\right)^2}} = \sqrt{\frac{j\left(\frac{\omega}{\omega_c}\right) \frac{\rho_{el}}{\rho_{ion} t_h^2} + \left(\frac{\omega}{\omega_c}\right)^2 \frac{\rho_{el}}{\rho_{ion} t_h^2}}{1 + \left(\frac{\omega}{\omega_c}\right)^2}} \quad (S25)$$

212 When  $\omega < \omega_c$ , the term  $\left(\frac{\omega}{\omega_c}\right)^2$  decays more rapidly than its linear counterpart  $\left(\frac{\omega}{\omega_c}\right)$ , giving the low-

213 frequency limit  $\gamma_{LF}$  for the propagation constant in Eq. 7:

214 
$$\gamma_{LF} = \sqrt{j\left(\frac{\omega}{\omega_c}\right) \frac{\rho_{el}}{\rho_{ion} t_h^2}} = \sqrt{j\omega c_v \rho_{el}} \quad (S26)$$

215 It follows

216 
$$\alpha_{LF}(\omega) = \sqrt{\frac{\omega c_v}{2\sigma_{el}}}; \quad v_{phase,LF}(\omega) = \sqrt{\frac{2\omega\sigma_{el}}{c_v}} \quad (S27)$$

217 considering the ionic and electronic conductivities  $\sigma_{ion} = 1/\rho_{ion}$  and  $\sigma_{el} = 1/\rho_{el}$ .

218 On the other hand, when  $\omega > \omega_c$ , we can replace Eq. S25 with

219 
$$\gamma_{HF} = \sqrt{\frac{j\left(\frac{\omega}{\omega_c}\right) \frac{\rho_{el}}{\rho_{ion} t_h^2} + \left(\frac{\omega}{\omega_c}\right)^2 \frac{\rho_{el}}{\rho_{ion} t_h^2}}{\left(\frac{\omega}{\omega_c}\right)^2}} = \sqrt{\frac{\rho_{el}}{\rho_{ion} t_h^2} + j \frac{1}{\left(\frac{\omega}{\omega_c}\right)^2} \frac{\rho_{el}}{\rho_{ion} t_h^2}} \quad (S28)$$

220 which can be simplified considering the limit

$$\begin{aligned}
221 \quad \lim_{a \gg b} (\sqrt{a + jb}) &= \lim_{a \gg b} [(\sqrt{z(\cos \varphi + j \sin \varphi)})] \\
222 \quad &= \lim_{a \gg b} \left\{ \sqrt{\sqrt{a^2 + b^2} \left[ \cos \left( \tan^{-1} \frac{b}{a} \right) + j \sin \left( \tan^{-1} \frac{b}{a} \right) \right]} \right\} \\
223 \quad &= \lim_{a \gg b} \left\{ \sqrt{a} \left( \cos \frac{b}{2a} + j \sin \frac{b}{2a} \right) \right\} = \sqrt{a} \left( 1 + j \frac{b}{2a} \right) \quad (\text{S29})
\end{aligned}$$

224 We obtain

$$225 \quad \gamma_{HF} = \sqrt{\frac{\rho_{el}}{\rho_{ion} t_h^2}} + j \frac{\sqrt{\rho_e}}{2\omega c_v \rho_i^{3/2} t_h^3} \quad (\text{S30})$$

226 which gives

$$227 \quad \alpha_{HF}(\omega) = \sqrt{\frac{\sigma_{ion}}{\sigma_{el} t^2}}; \quad v_{phase, HF}(\omega) = \frac{2\omega^2 \sqrt{\sigma_{el} c_v} t^3}{\sigma_{ion}^{3/2}} \quad (\text{S31})$$

228

229

230

231

232

233

234

235

236

237

238

239

240

241

242

243

244

245 **7. Electrical properties of neural axons**

246

247 Table S1 reports the electrical properties of neural axons used for the simulations in Figure 5a  
248 and 5b:<sup>3</sup>

249

	<b>Axon</b>	<b>Myelinated axon</b>
$\sigma$ (S/m)	3	30
$c$ (F/m <sup>2</sup> )	0.1	0.01
$r$ (mm)	0.5	0.5

250

251

252

253

254 **Table S1:** Conductivity, superficial capacitance, and radius of neural axons.

255

256

257

258

259

260

261

262

263

264

265

266

267 **References:**

268 1. Hayt, W. H. *Engineering Electromagnetics*. (New York : McGraw-Hill, 1989).

269 2. de Levie, R. On porous electrodes in electrolyte solutions: I. Capacitance effects.  
270 *Electrochimica Acta* **8**, 751–780 (1963).

271 3. Nelson, P. C. & Nelson, P. *Biological Physics*. (WH Freeman New York, 2004).

272